Nanoscale dielectric properties of TiO2 in SiO2 nanocomposite deposited by hybrid PECVD method

C Villeneuve-Faure, Maria Mitronika, A P Dan, Laurent Boudou, William Ravisy, M P Besland, Mireille Richard-Plouet, Antoine Goullet

Nano Express

PAPER • **OPEN ACCESS**

Nanoscale dielectric properties of TiO_2 in SiO_2 nanocomposite deposited by hybrid PECVD method

To cite this article: C Villeneuve-Faure *et al* 2024 *Nano Ex.* **5** 015010

NANO EXPRESS

OPEN ACCESS

RECEIVED
18 September 2023

REVISED
12 January 2024

ACCEPTED FOR PUBLICATION
23 January 2024

PUBLISHED
7 February 2024

PAPER

Nanoscale dielectric properties of TiO_2 in SiO_2 nanocomposite deposited by hybrid PECVD method

C Villeneuve-Faure[1], M Mitronika[2], A P Dan[1], L Boudou[1], W Ravisy[2], M P Besland[2], M Richard-Plouet[2] and A Goullet[2]

[1] LAPLACE (Laboratoire Plasma et Conversion d'Energie); Université de Toulouse; CNRS, UPS, INPT; 118 route de Narbonne, F-31062 Toulouse cedex 9, France

[2] Université de Nantes, CNRS, Institut des Matériaux Jean Rouxel, IMN, F-44000 Nantes, France

E-mail: christina.villeneuve@laplace.univ-tlse.fr

Keywords: TiO_2–SiO_2 nanocomposite thin films, atomic force microscopy, low-pressure plasma processing, dielectric thin films

Abstract

In this paper, nanocomposites (TiO_2 in SiO_2) are produced by an advanced hybrid aerosol-PECVD method based on direct liquid injection of a non-commercial colloidal solution in an O_2 / hexamethyldisiloxane (HMDSO) low-pressure plasma. Dielectric properties are investigated at nanoscale using techniques derived from Atomic Force Microcopy in terms of relative dielectric permittivity, charge injection and transport. Results show that a concentration in TiO_2 up to 14% by volume makes it possible to increase the relative dielectric permittivity up to 4.8 while maintaining the insulating properties of the silica matrix. For a TiO_2 concentration in the range 15%–37% by volume, the relative dielectric permittivity increases (up to 11 for 37% TiO_2 by volume) and only few agglomerated nanoparticles lowering the insulating properties are observed. For TiO_2 concentration above 40% by volume, the relative dielectric permittivity still increases but the quantity of agglomerated nanoparticles is very high, which greatly increases the charge transport dynamic and degrades the insulating properties. Finally, 37% of TiO_2 by volume in the SiO_2 matrix appears to be the best compromise, between high dielectric permittivity and low leakage current for the MIM applications aimed.

1. Introduction

In microelectronic devices, dielectric materials are widely used for passive or active functions. In addition, Metal-Insulator-Metal (MIM) structures are part of many devices such as analog-to-digital converters, DC voltage decoupling, dynamic random-access memory. Main requirements on dielectric materials for such devices are high energy storage density, low dissipation factor and high temperature stability [1, 2]. Among dielectrics, silicon dioxide (SiO_2) thin films meet several criteria for MIM structures, such as low leakage current and high energy storage but exhibit a strong limitation due to a low relative dielectric permittivity (ε_r) [3]. The projection of International Roadmap for Devices and Systems (IRDS) 2026 for MIM structures highlights the need for an equivalent oxide thickness (EOT) close to 1 nm, a relative dielectric permittivity ε_r greater than 40 and a leakage current lower than 10^{-8} A cm^{-12}. To fulfil these requirements, the relative dielectric permittivity should increase and/or the layer thickness decrease leading to breakdown strength reduction and capacitance quadratic voltage coefficient increase, which is not favorable for the applications [1]. To overcome this disadvantage, several materials have been investigated. First, high-k materials such as TiO_2, HfO_2, $BaTiO_3$ or Al_2O_3 were identified as the most promising candidates to improve MIM performances [1, 4, 5]. Indeed, compared to SiO_2, these oxides exhibit the same capacitance density for thicker dielectric film which minimizes the leakage current generated by tunneling mechanisms. However, MIM capacitors based on high-*k* materials exhibit also leakage currents due to their weak dielectric strength [6, 7]. To avoid this behavior, mixed oxides such as $Ti_xSi_{1-x}O_2$ have been developed. However, $Ti_xSi_{1-x}O_2$ films which exhibit low leakage current do not offer enough increase of their dielectric permittivity increase [8]. In a second approach, high-k multilayers

stacking or nanolaminates were investigated since they lead to a reduction in leakage current and an increase in ε_r which depends on the number of layers [1]. Studies on various dielectric stacks are reported in the literature, mainly developed by Atomic Layer Deposition (ALD), as TiO_2-Al_2O_3 [9], HfO_2-Al_2O_3 [10], VO_2-SiO_2 [11], Ta_2O_5-HfO_2 [12], ZrO_2-HfO_2 [12], Ta_2O_5-ZrO_2 [12], HfO_2-SiO_2 [13] or ZrO_2-La_2O_3 [14]. These stacks associate layers of high-k materials with highly insulating ones as SiO_2 or Al_2O_3 [15]. In the case of TiO_2-Al_2O_3 nanolaminates, it was demonstrated that a reduction of the lower layer thickness led to an increase of ε_r and dielectric loss (i.e. conductivity). The best compromise was obtained for a 3.8 nm-thick sublayer (ε_r around 30 and dielectric loss around of 0.5 at 100 Hz) [9]. This apparent ε_r enhancement, observed in various nanolaminates, is not only related to the permittivity of the involved materials but also to physical phenomena occurring at the interfaces such as charges accumulation by Maxwell–Wagner-type dielectric relaxation [9, 15, 16] or chemical modifications [9–15]. Moreover, for many nanolaminates, dielectric properties improvement need high-temperature post-deposition annealing (i.e. up to 700 °C–800 °C) [12–15] that could be a limitation for the integration in microelectronic devices. A third approach based on Nanocomposites (NC) appears promising, since results on nanolaminates demonstrate that interfaces have a strong influence on relative dielectric permittivity increasing [15]. Indeed, NC make it possible to increase the number of interfaces and to control their properties thanks to nanoparticles surface treatment. Thin polymer NC based on TiO_2 or ZnO high-k nanoparticles (NPs) were successfully used in Organic field-effect transistor (OFET) to improve performances in term of field-induced current [17]. However, to our knowledge, MIM structures based on fully-inorganic NC materials are barely reported in the literature. Y. Sun *et al* reported on VO_2/SiO_2 NC for thermally tunable capacitor leading to a leakage current lower by three orders of magnitude than that obtained for a VO_2/SiO_2 multilayer structure but associated with a reduced capacitance density [11].

In this context, our aim is to investigate the dielectric properties of a fully-inorganic NC material with TiO_2 nanoparticles (NPs) in a SiO_2 matrix in order to take advantage of the best properties of each material. Indeed, TiO_2 exhibits a high relative dielectric permittivity (up to 80) [18] and SiO_2 shows a low leakage current (less than $1.\ 10^{-8}$ A.cm^{-2} for an electric field of 250 V.m^{-1}) [18]. Several chemical and physical methods have been developed to synthesize such NC films. Considering the sol–gel method, the main drawback to elaborate NC is the need of several steps and the possible toxicity of handling NPs during the drying step [19]. Plasma enhanced chemical vapor deposition (PECVD), chemical vapor deposition (CVD) or hybrid sputtering-PECVD have also demonstrated their ability to synthesize NC thin films [20–22]. More recently, an advanced hybrid aerosol-PECVD method based on direct liquid injection of a colloidal solution in an O_2 / hexamethyldisiloxane (HMDSO) low-pressure plasma to form TiO_2 in SiO_2 [23, 24] or ZnO in SiO_2 [25] NC films has been developed. Moreover, the injection of colloidal solutions avoids any handling of NPs and the process can thus be considered as environmentally friendly and safe-by-design. Another advantage of this process is the control of nanoparticles/matrix interfaces thanks to the colloidal solution. In addition, this includes the ability to modify the interface properties and offer an accurate control of dielectric properties.

In this context, we aim to develop thin films with tunable properties of a fully-inorganic nanocomposite (i.e. TiO_2 NPs in SiO_2) elaborated at low temperature by a safe-by-design process. In this paper, we investigate the dielectric properties of the TiO_2 in SiO_2 NC films elaborated by such hybrid aerosol-PECVD method. The effect of the TiO_2 fraction incorporated in the SiO_2 matrix on the morphology and dielectric properties (dielectric permittivity, charges injection and transport) of the deposited films is investigated. Electrical properties are studied at nanoscale using techniques derived from Atomic Force Microscopy (AFM) to improve understanding of NPs influence at local scale. The main objective is to determine the optimal TiO_2 fraction by volume that leads to the best compromise, i.e. highest dielectric permittivity and lowest leakage current.

2. Experiments

2.1. Nanocomposite thin film preparation

The TiO_2–SiO_2 NC thin films were prepared by a hybrid process combining low pressure PECVD for the deposition of the SiO_2 matrix and controlled injection of very stable TiO_2 colloidal solution [23]. As stated in previous work [24, 26], due to the synthesis conditions, solvent molecules act as stabilizing ligands around the particles allowing the solution to remain stable for years. In order to produce a totally inorganic amorphous silica matrix [27], a high-density inductively coupled plasma (ICP) created at 13.56 MHz was ignited by applying a power discharge of 400 W to a gaseous mixture including O_2 95%-Ar 5%: 24 sccm and HMDSO: 0.11 sccm. No intentional heating of the substrate is required to remove the ligands and mineralize the NPs surface by interaction between the droplets of solution drying at the substrate surface and the plasma [28]. As reported, the volume fraction of TiO_2 NPs can be tuned by the TiO_2 precursor injection N within a sequence of 1 min. The pulsed injection is made at a frequency of 0.5 Hz and 1 ms injection time in order to limit any plasma pressure

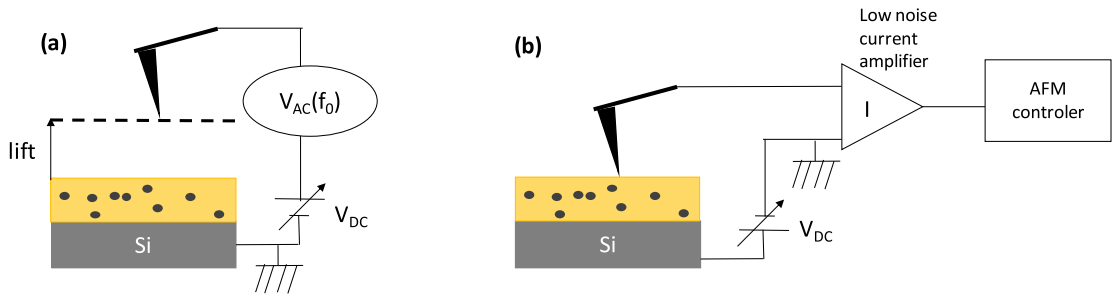

Figure 1. Simplified scheme of AFM setup in (a) EFM/KPFM and (b) C-AFM configurations.

variations. Such sequence is repeated until the targeted thickness is reached (50 nm in this study). For the present work, we present results on NCs thin films obtained for N = 1, 5, 10, 20 and 30.

2.2. Structural and surface characterization

Atomic Force Microscopy (AFM) was used in tapping mode with a Bruker Multimode 8 setup to characterize the surface morphology. Some selected samples were deposited on Indium-doped Tin oxide (ITO) on polyethylene terephthalate (ITO (50 nm) / PET (125 μm), Sheldahl) for observations by Transmission Electron Microscopy (TEM) (S/TEM Themis ZG3, 300 kV, Thermo Fisher Scientific). High resolution TEM images were obtained on cross-sections prepared by ultramicrotome (Leica UC7/FC7) equipped with diamond knife (Diatome).

The NC thickness, composition and optical properties were investigated by spectroscopic ellipsometry. The *in situ* real time accurate monitoring of the films growth was carried out with a rotating compensator spectroscopic ellipsometer (J.A. Woollam M- 2000) mounted on the plasma reactor. Measurements were conducted between 250 and 1000 nm at 72° incident angle in order to control the film growth and to extract film composition and thickness. To fit the ellipsometric data, a similar procedure as the one previously reported has been involved [23]. A two-phase material (SiO_2 and TiO_2) was set up to account for the ellipsometric data of the TiO_2-SiO_2 NC thin film. The Bruggeman Effective Medium Approximation (BEMA) was thus used to model the TiO_2 NPs dispersed in the SiO_2 matrix that was accounted for using the Cauchy dispersion law whereas the Tauc-Lorentz dispersion law was used for the TiO_2 NPs.

2.3. Nanoscale electrical characterizations

Nanoscale electrical characterizations were carried out on a Bruker Multimode 8 setup using three different modes: Electrostatic Force Microscopy (EFM) for the dielectric permittivity [29, 30], Kelvin Probe Force Microscopy (KPFM) for the charge injection and trapping dynamics [31] and the Conductive AFM (C-AFM) for the current flowing through the NC films [32]. Experimental setups are described in figure 1.

EFM measurements were done using Pt-coated Si-tip with resonance frequency f_0 of 75.5 kHz, a quality factor Q of 293, a curvature radius R_c of 25 nm and a spring constant k of 2.81 N m^{-1}. EFM measurement of the resonance phase shift $\Delta\phi_0$ was done at 20 nm-lift with an applied potential on the tip V_{DC} equal to 0 V or 5 V (figure 1(a)). The resulting experimental phase shift parameter $a_{\Delta\phi}$ is determined using the following equation:

$$a_{\Delta\phi} = \frac{\Delta\phi_0(5V) - \Delta\phi_0(0V)}{5^2 - 0^2} \quad (1)$$

This methodology allows taking into account a reference phase shift that corresponds to 0 V applied to the tip.

From a theoretical point of view, the resonance phase shift $a_{\Delta\phi}$ is related to the capacitance C between AFM probe and the sample by [29]:

$$a_{\Delta\phi} = \frac{Q}{2k}.\frac{d^2C}{dz^2} \quad (2)$$

where z is the vertical distance, Q the quality factor and k the stiffness of the cantilever.

The quantity d^2C/dz^2 is determined by using a 2D axisymmetric Finite Elements Model developed with COMSOL [30], in which the electrostatic force F_e is computed at different lift positions and for different dielectric permittivity values. This modelling approach allows to extract a theoretical non-linear relationship between the relative dielectric permittivity ε_r and $a_{\Delta\phi}$ parameter. Finally, this relationship is applied to the $a_{\Delta\phi}$ experimental map (equation (1)) which permits to obtain the relative dielectric permittivity distribution at nanoscale. This model was calibrated using two well-known samples as reference: 50 nm-thick pure SiO_2 and TiO_2 layer deposited on highly-doped Si substrate whose dielectric permittivity has been determined by dielectric spectroscopy.

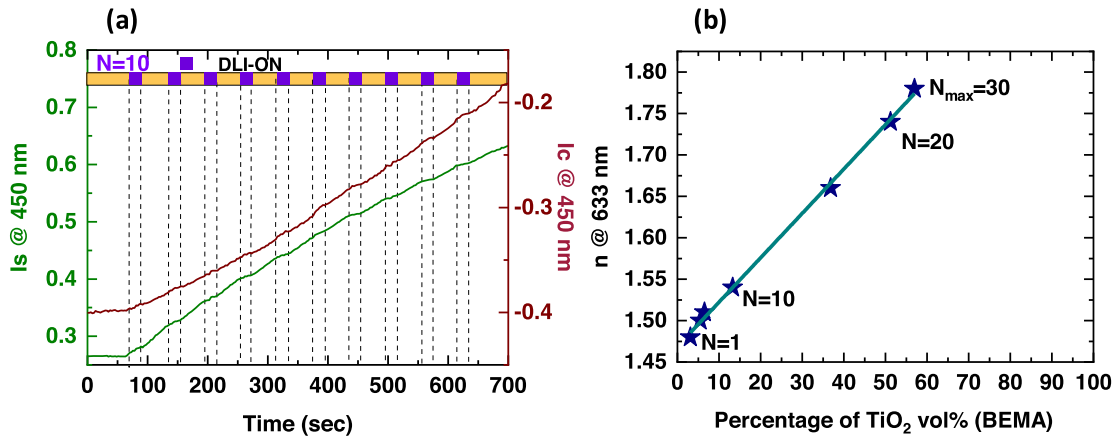

Figure 2. (a) *In situ* dynamical ellipsometry Is (left hand-side *y*-axis), Ic (right hand-side *y*-axis) parameters at 450 nm measured during the first 10 min of the liquid injection N = 10. Each minute corresponds to one sequence. In the top bar, with purple is notified the injection ON period (T_{ON} = 20 s) and with orange the injection OFF part (T_{OFF} = 40 s). (b) Effective refractive index at 633 nm extracted from the Bruggeman Effective Medium Approximation (BEMA) for varying injection parameter N as a function of the volume TiO_2 percentage in the silica matrix (adapted from [23]).

Charge injection and trapping dynamics were investigated by KPFM under controlled atmosphere (without humidity and under N_2 gas), to avoid charges dissipation due to a layer of water on the sample surface. The charging step was achieved in contact mode (contact force set to around 40 nN to ensure tip-coating integrity) by applying positive or negative DC bias (V_{DC} from −40 V to +40 V by step of 10 V) to the AFM tip for 1 min with sample back side grounded. After this charging step, the same tip was used to probe the surface potential in Amplitude Modulation KPFM (AM-KPFM) mode using a lift of 50 nm. For surface potential measurement and charges injection protocol, a Pt-coated Si-tip is used (R_c = 25 nm and f_0 = 77.5 kHz). The investigated area of the sample surface is different for each charge injection and AM-KPFM measurement, in order to insure a region free of charge before measurements and thus avoid the influence of previous trapped charges.

Current measurements at nanoscale were investigated by C-AFM using a Pt/Ir coated Si-tip (R_c = 28 nm and k = 0.42 N m^{-1}) with different low noise amplifier modules: from low current module (from 1 pA to 200 pA) for lowest conductive area to middle range current module (from 100 pA to 10 nA) for highest conductive area. As described in figure 1(b), the AFM tip plays the role of a top electrode and collects the current within the NC layer. Various bias voltages V_{DC} were applied to the NCs thin films in the −40 V to + 40 V range and a contact force of around 35 nN was maintained during current measurement.

3. Results

3.1. Structural and surface morphology characterization

As a first step of this study, the NC layer growth is followed by *in situ* ellipsometry as shown in figure 2(a) with the Is/Ic trajectory plots at a constant wavelength of 450 nm. The dynamical monitoring of the experimental Is and Ic curves for the 10 first minutes of the growth clearly shows the two different zones associated to each sequence (DLI-ON and DLI-OFF). For each DLI ON duration, one can observe a strong decrease of the slope for both Is and Ic. Indeed, though the injector is controlled to limit the pressure increase during T_{ON}, the plasma density and consequently the deposition rate are strongly reduced. During the DLI-ON time mainly NPs are deposited whereas the HMDSO vapor dissociation is not efficient (nevertheless a small amount of SiO_2 growth takes place). On the contrary, during the DLI-OFF the SiO_2 matrix is efficiently deposited without TiO_2 NPs. Generally, from this dynamic study, it appears that in all cases (N = 1 to 30) the total evolution of the Is and Ic curves is similar for the first 10 min of growth. With an average growth rate of 1.4 nm.min^{-1} (N = 10), these results clearly reveal that measurement resolution corresponds to about 0.2 nm film thickness variation and confirms that *in situ* ellipsometry is a very accurate tool to control the growth. This alternating mode of deposition is also a way to tune precisely the film composition. This means that as N is increased, the content of the TiO_2 NPs increases and that of SiO_2 decreases.

At the end of each deposition, the effective refractive index of the TiO_2/SiO_2 NC films has been extracted using the Bruggeman Effective Medium Approximation (BEMA) [23]. The optical film effective index at 633 nm is plotted in figure 2(b) as a function of the volume fraction of the TiO_2 NPs distributed in the SiO_2 matrix for an increasing N parameter. At N = 1, the fraction of NPs has a value of 2.5 vol% and an effective refractive index of 1.48. For N = 30, the fraction increases up to 58 vol%, with an effective refractive index of 1.78. From these

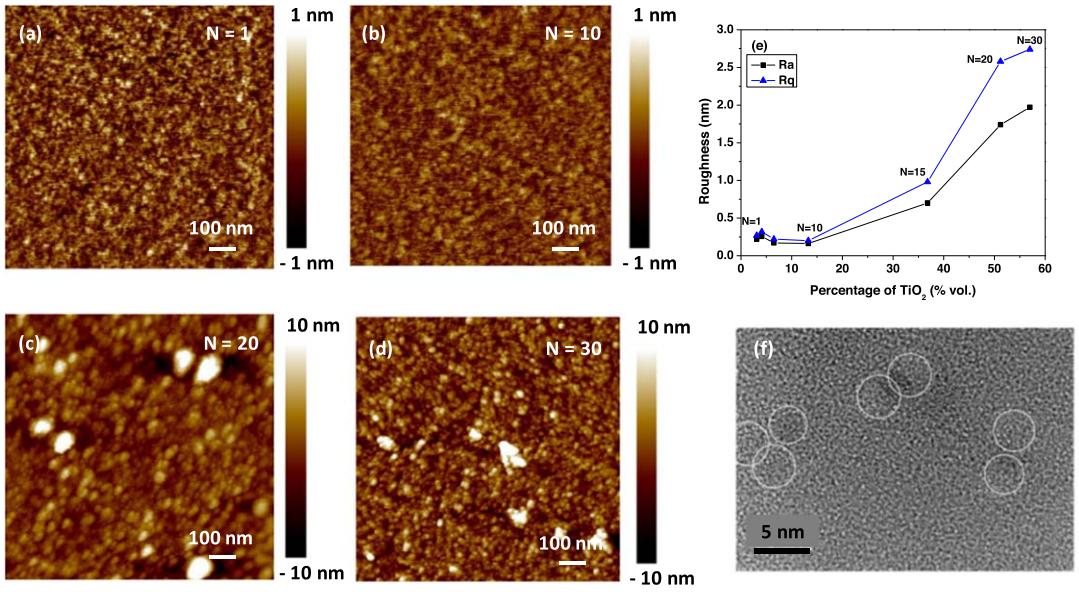

Figure 3. AFM surface topography of NC films for (a) N = 1, (b) N = 10, (c) N = 20 and (d) N = 30. (e) Evolution of arithmetic Ra and root mean square Rq surface roughness with percentage of TiO_2 over 1 μm × 1 μm probed area. (f) Typical HRTEM image of a NCs thin film obtained with N = 10, showing the incorporation of crystalline TiO_2 NPs, smaller than 5 nm in diameter, dispersed in the silica matrix. The spherical edges are highlighted by white circles.

results, we observe a very accurate control of the NC composition and effective optical index by the deposition conditions. Indeed, a very good trend of linear increase of the index with the TiO_2 content is observed from 1.47 (SiO_2 optical index) to 1.78 when the volume fraction of TiO_2 NPs varies from zero (100% SiO_2) to 58 (42% SiO_2). It is worth noting that the extrapolated n index slightly differs from the one expected for anatase bulk phase. Indeed, the refractive index is still higher than the index found for the plasma treated NPs [28]. Nevertheless, the refractive index has lower values than the ones obtained for bulk, plasma- deposited TiO_2 films (n = 2.3 at 633 nm) due to the nanometer size of TiO_2 NPs in the film deposited by hybrid PECVD method. This is consistent with the optical gap value determined at 2.4 eV, whatever the N value. In addition, it is to highlight that our ellipsometric model assumes that the TiO_2 NPS are homogeneously dispersed in the film. In order to check this hypothesis, complementary AFM/TEM analysis were performed.

Surface morphology and topography of the deposited TiO_2 in SiO_2 nanocomposite thin films were investigated by AFM as reported in figure 3. From AFM images, the arithmetic average Ra and the root mean square Rq of the 3D roughness were extracted. For $N \leqslant 10$, the amount of TiO_2 NPs has no influence on the surface morphology (figures 3(a) and (b)) and the roughness value is much lower than 0.5 nm (figure 3(e)), i.e. a value similar to the one of SiO_2 films [8]. As shown in a typical high resolution TEM image (figure 3(f)), crystalline TiO_2 nanoparticles, embedded in amorphous silica matrix, are clearly identified (i.e. white circles). In addition, previous results highlighted that the process does not modify the crystalline nature of nanoparticles [23]. In this image, it is worth noting that 2 or 3 NPs are agglomerated together. However, TiO_2 NPs remain mostly individualized and no significant agglomeration was observed. Moreover, this observation emphasizes that the TiO_2 nanoparticles present an average diameter of 4 nm. These results highlight that the introduction of TiO_2 NPs does not modify the surface morphology up to 15% by volume. Above this value, the roughness remains low and in the same order of magnitude than the TiO_2 nanoparticles diameter. For $N > 10$, the surface morphology appears modified (figures 3(c) and (d)) and larger grains are observed on the surface and their occurrence increases with N which implies a surface roughness increasing (figure 3(e)) although limited to 3 nm. Moreover, the lateral dimension of these objects (i.e. 50–100 nm) is larger than nanoparticles ones (i.e. 4 nm). So, this phenomenon, not observed for bare SiO_2, is related to the interaction between the colloidal solution and the plasma. Indeed, increasing N means that the injector (for the TiO_2 solution) is open more often allowing thus the incorporation of a larger amount of solution and thus increase of TiO_2 content injected per minute. This increase of colloidal solution in the plasma could modified the matrix properties. Consequently, the surface morphology and roughness of the deposited films are mainly driven by the amount of colloidal solution injected in the plasma (i.e. the amount of TiO_2 NPs). However, even if the surface roughness is increased as compared to lower value of N (figure 3(d)), it remains below 4 nm (i.e. nanoparticles size). When compared to literature, this NC surface roughness is of the same order of magnitude as SiO_2-TiO_2 nanolaminates processed by ALD for optical applications [33].

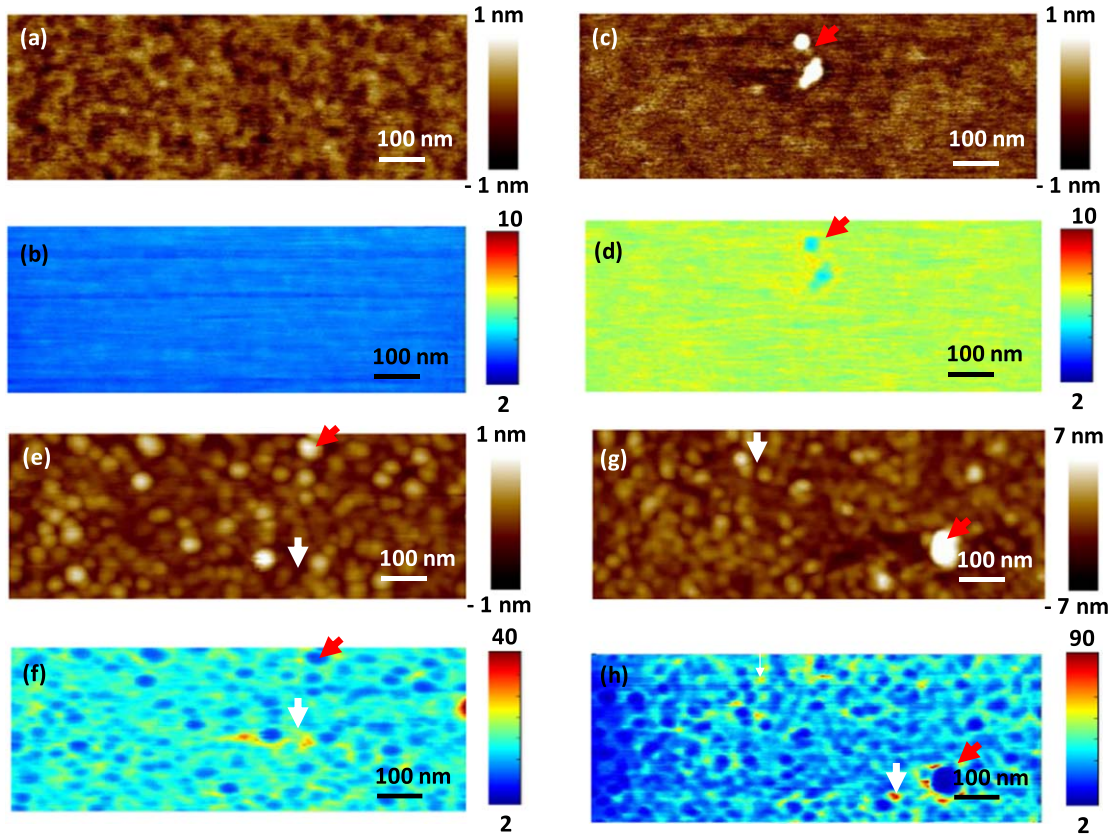

Figure 4. EFM (a,c,e,g) surface topography and (b,d,f,h) relative dielectric permittivity ε_r mapping analysis for (a,b) N = 1, (c,d) N = 10 (e,f) N = 20 and (g,h) N = 30 nanocomposite films. Red arrows indicate SiO_2 rich area and white arrows TiO_2 rich area.

3.2. Dielectric permittivity characterization

In figure 4, AFM images show topography and relative dielectric permittivity maps obtained by EFM for TiO_2 in SiO_2 NC films. Concerning the relative dielectric permittivity, the mean value and standard deviation, over the map, are determined to identify the NPs dispersion. For N = 1, the dielectric surface topography is smooth (figure 4(a)) and the dielectric permittivity (figure 4(b)) appears homogeneous. The main value is around 3.75 ± 0.1, which is close to SiO_2 one [8]. Hence, no TiO_2 NPs are observed. For N = 10, the dielectric surface topography remains smooth and two different grain-like structures are observed (red arrow on figure 4(c)). The corresponding relative dielectric permittivity map appears quite homogeneous with a main value around 4.7 ± 0.3. Therefore, the presence of TiO_2 NPs increases the apparent dielectric permittivity even if no NP is detected close to the surface. The grain-like structures (red arrow on figure 4(d)) present a relative dielectric permittivity close to 3.8, which implies that such grains correspond to SiO_2-like area. For N = 20, the dielectric surface topography (figure 4(e)) presents a lot of grains that is consistent with the higher surface roughness observed in tapping mode (figure 3(e)). The corresponding relative dielectric permittivity map (figure 4(f)) is no more homogeneous and associated to high permittivity area (white arrow) which correspond to TiO_2-rich area (less than 30 nm in lateral size) and low permittivity area (red arrow) with a permittivity close to 3.8 that can be associated to SiO_2-rich area. As the lateral dimension of the TiO_2 NPs is in the 4 nm range, the TiO_2-rich area might be associated to agglomerates of NPs. The main dielectric value is close to 15.5 ± 0.3. The results obtained for N = 30 are similar to the ones obtained for N = 20 with an heterogeneous surface topography (figure 4(g)) exhibiting similar grain size and relative dielectric permittivity map (figure 4(h)). In that case, TiO_2-rich area (white arrow) and SiO_2-rich area are observed. Due to the TiO_2 fraction by volume, the average value of permittivity is increased up to 29.5 ± 0.6.

Dielectric permittivity determination by EFM can be modified by three main parameters. *(i)* Error due to AFM tip parameters used in the finite element model. In this study, the calibration on SiO_2 and TiO_2 well-known layers, as references, allows to avoid this shortcoming. *(ii)* Thickness variation mainly due to surface roughness as reported in literature [34, 35]. Considering NC investigated in this study (figure 2), the highest variation of the NC thickness due to surface topography is of 6%. Such thickness variation would generate a variation of 1.5% on the dielectric permittivity value. *(iii)* Noise on EFM phase shift measurement is determined

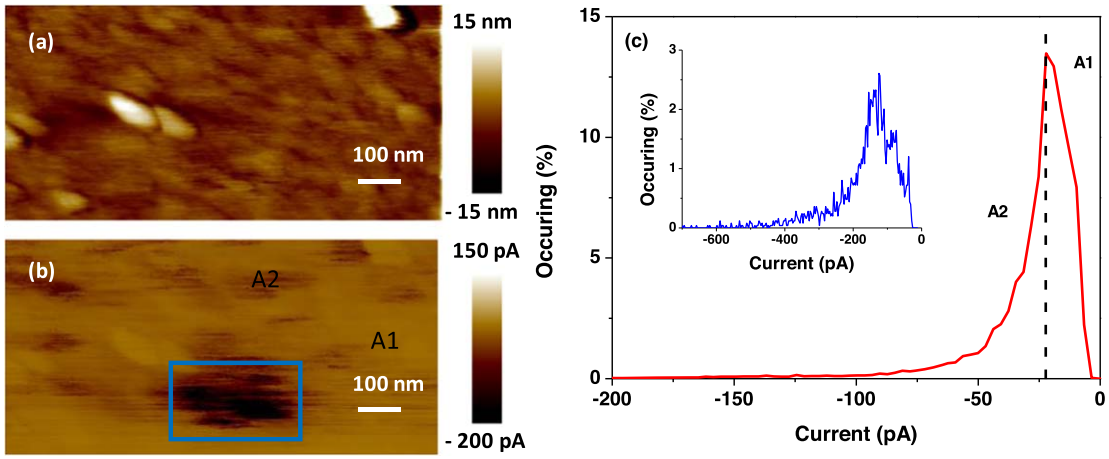

Figure 5. (a) Topography and (b) current map in C-AFM mode for −18 V applied on N = 30 nanocomposite film. (c) Occurring diagram corresponding to the current map. Inset. Occurring diagram for the area in the blue square.

on the silica reference sample, and correspond to a variation of 2% in the dielectric permittivity. Consequently, he maximum error would be of 3.5% that is similar to the dispersion range observed in NC dielectric map.

As expected, the mean value of the relative dielectric permittivity increases with the content of TiO_2 nanoparticles (i.e. N parameter). For $N \leqslant 10$, the relative dielectric permittivity map appears homogeneous and no TiO_2 NPs are observed. For $N > 10$, the relative dielectric permittivity map appears heterogeneous and SiO_2-rich and TiO_2-rich areas are evidenced.

3.3. Charge injection and transport

Finally, to get more insights in the electrical properties of TiO_2 in SiO_2 nanocomposite films, charges injection and transport at local scale were investigated by AM-KPFM and C-AFM modes, respectively.

Figures 5(a) and (b) show surface topography and associated current maps for a −18 V bias applied on the N = 30 NC film obtained by C-AFM. In figure 5(c), the diagram shows the statistical distribution of the current value over the entire analyzed area. As for the relative dielectric permittivity map, the current through the NC film is not homogeneous over the whole surface and 3 different areas are identified. A low current area, so-called A1, which represents around 60% of the surface and exhibits a current value ranging from −5 pA to −25 pA. A medium current area, so-called A2, which represents nearby 34% of the surface, exhibits a current value ranging from −25 pA to −200 pA. A high current area (blue rectangle) represents 6% of the surface and exhibits a current ranging from −100 pA to −600 pA (figure 5(c) inset). This area could be related to the presence of TiO_2 nanoparticles agglomerates (i.e. high dielectric permittivity area on figure 3(h)) with a significant conductivity for negative carrier [8]. Moreover, no peak is observed at 0 pA, meaning that the current is measurable (i.e. higher than 0.1 pA) for all analyzed surface. Concerning N = 20 nanocomposite film, only 10% of the surface is conductive and a current value close to −20 pA is achieved for −28 V applied on the substrate. These regions might be associated to TiO_2-rich areas since they exhibit high dielectric permittivity (as shown in figure 4(f)). For nanocomposite with $N \leqslant 15$ no current was measured for all applied voltage. Moreover, for all analyzed nanocomposite film, no current was measured for positive applied bias. We assume that this could be probably due to the N-type nature of the TiO_2.

In AM-KPFM configuration, charges were injected by applying a positive or a negative bias to the tip, whereas the Si substrate was grounded. For N = 1 NC film, a comparison between surface topography (figure 6(a)) and surface potential (figure 6(b)), after charge injection (1 min at 20 V), emphasizes no modification of the topography induced by the injected charge. Moreover, the surface potential exhibits a conventional round-like shape with a cross-section (red line on figure 6(b)) exhibiting a bell-like shape profile (inset figure 6(d)). Rather similar behavior is observed for $N \leqslant 10$. For N = 15 nanocomposite films, the surface topography is not influenced by injected charge (figure 6(c)) as for all studied samples, but the surface potential is no more round-like shaped (figure 6(d)). Therefore, TiO_2 NPs dispersed in the SiO_2 layer influenced the charge injection. The influence of NPs on injected charge cloud has been already observed in the case of silicon nanocrystal embedded in a SiO_2 matrix [36] or SiO_2 nanoparticles in a Low Density Polyethylene (LDPE) matrix [37]. Moreover, the profile shape remains bell-like after charge injection (inset figure 6(d)). To fully understand such behavior, surface potential profiles were fitted with a Gaussian function to extract three parameters: *(i)* the maximum surface potential V_m, *(ii)* the Full-Width at Half Maximum (FWHM) that represents the lateral charge spreading and *(iii)* the area under the potential peak A_s that represents the charge density for a fixed

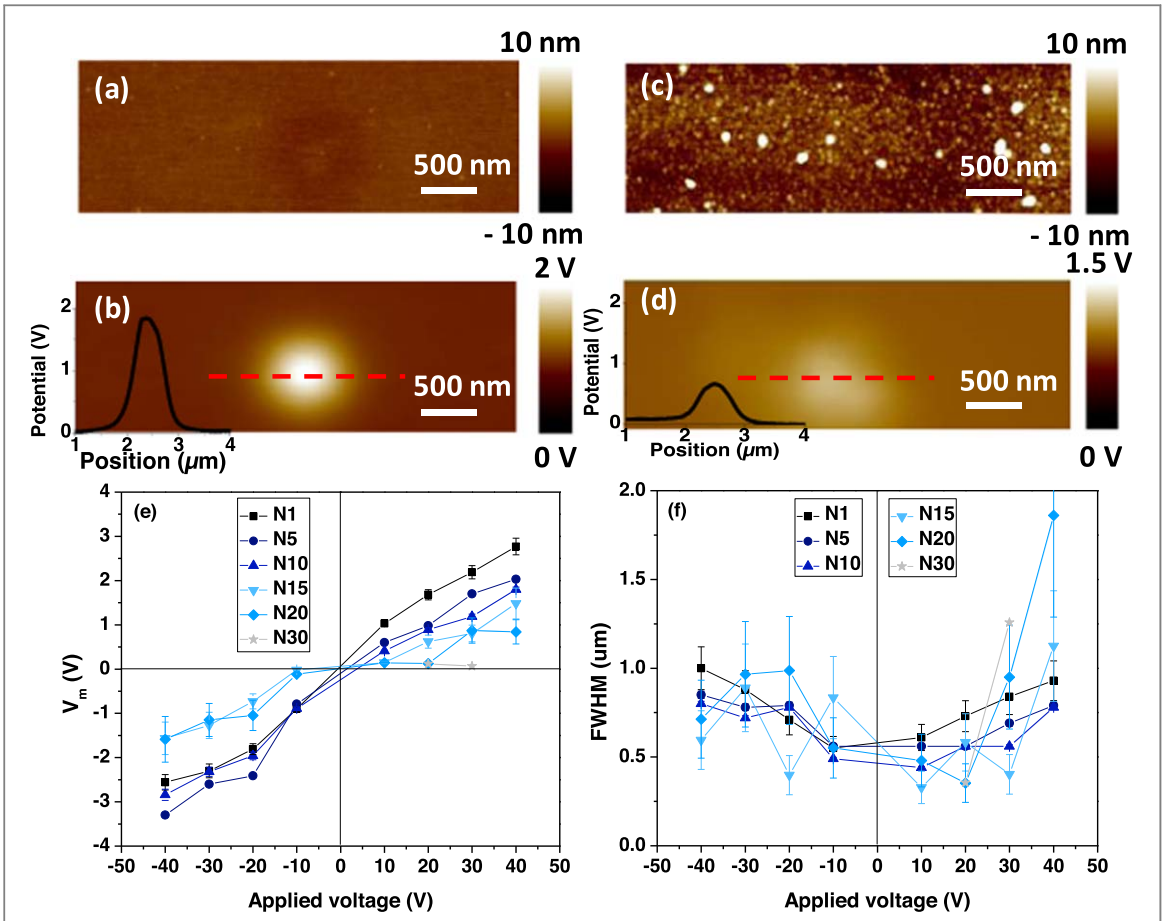

Figure 6. (a) Topography and (b) surface potential cartography after charge injection (1 min at 20 V) in N = 1 nanocomposite film. Inset: Surface potential profile along red dashed-line. (c) Topography and (d) surface potential cartography after charge injection (1 min at 20 V) in N = 15 nanocomposite film. Inset: Surface potential profile along red dashed-line. Evolution of (e) surface potential maximum V_m and (f) the FWHM as function of applied bias for different nanocomposite films.

thickness [38]. For each applied voltage, charge injection was carried out at three different locations on the film NC surface. Mean value and standard deviation of each parameter (V_m, FWHM and A_s) were determined to provide an assessment on dispersion. The evolutions of the surface potential maximum V_m and the FWHM are plotted as function of applied bias for charges injection in figures 6(e) and (f) respectively.

Concerning N = 1 NC films (black square symbol), both V_m and FWHM are increasing correspondingly with the applied bias that is consistent with the behavior observed for SiO_2 films [8, 38]. For N = 5 and N = 10 NC films, the same behavior as the one observed for N = 1 is obtained (i.e. a linear increase for both V_m and FWHM for the both polarities of the applied voltage). However, the slightly higher V_m measured for a negative bias as compared to a positive one is significant for a quantity of trapped charge slightly higher for negative carriers than for positive ones. Nevertheless, the standard deviation remains low (<5%) as nanoparticles are homogeneously dispersed in the silica matrix. For N = 15 and N = 20 NC films, V_m and FWHM are increased with the applied bias. As for N = 5 and N = 10, V_m is lower for positive bias than for negative one meaning that the amount of positive trapped charge is lower than negative ones. However, V_m remains lower than for $N \leqslant 10$ nanocomposite films, which implies a trapped charge quantity lower for N = 15 and N = 20 NC films as compared to $N \leqslant 10$ nanocomposite films. Moreover, the FWHM and V_m exhibit a higher standard deviation. The origin could be that the charge injection and transport are varying depending on the location of the charge cloud: either close to a nanoparticles agglomerate (high conductivity associated to higher FWHM and lower V_m) or in an area where NPs are widely dispersed behavior close to silica with lower FWHM and higher V_m). In the case of N = 30 no trapped charge is observed at negative bias that is consistent with the high current probed by C-AFM. For positive charges, a small amount of injected charges is observed at positive bias, but only for the lowest values (i.e. 10 V and 20 V). For all measurements, the amount of injected charge decreases as the TiO_2 NPs fraction by volume is increasing in the NC films. Finally, a behavior similar to the SiO_2 one is observed for a TiO_2 fraction below 15% by volume.

To analyze charge transport after injection, the maximum surface potential V_m and the potential profile FWHM were plotted as a function of the relaxation time for each layer. To emphasize charge dynamics,

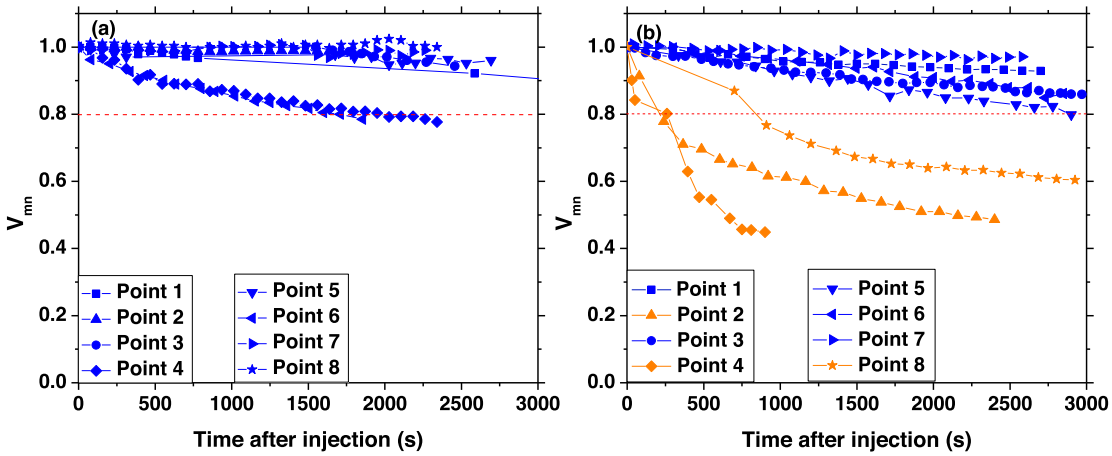

Figure 7. Evolution of the normalized surface potential maximum V_{mn} as a function of time after injection for different bias values for N = 1 (a) and N = 15 (b). Blue curves are associated to SiO_2-like behavior and orange curve to TiO_2 agglomerates.

normalized values are given as a function of time: *(i)* Normalized maximum potential V_{mn} that corresponds to surface potential maximum at time t after injection divided by the initial maximum value. *(ii)* Peak broadening ΔW that corresponds to the difference between FWHM at time t and at t = 0 s. For all amounts of TiO_2 NPs in the SiO_2 matrix, the peak broadening ΔW is not significant versus time after charge injection, meaning that charge lateral dispersion is not involved in the charge relaxation process. To take into account the spatial heterogeneity of the NC films (figure 4 and figure 5), charge transport dynamics were investigated with 8 points randomly distributed on the surface. Figure 7(a) represents the evolution of the normalized surface potential maximum V_{mn} as a function of time for N = 1 NC film. For all locations, the V_{mn} slowly decreases with a dynamic similar to the one of SiO_2 films [8, 38]. The same decreasing behavior is observed for N = 5 and N = 10 NC films. Consequently, TiO_2 in SiO_2 NC films with $N \leqslant 10$ exhibit similar insulating properties that SiO_2 i.e. a strong charge retention. For N = 15, a different behavior is observed (figure 7(b)). Two charge transport phenomena are observed: *(i)* a slow decrease of V_{mn} versus time after injection with a kinetic similar to N = 1 and SiO_2 films (blues curves in figure 7(b)). The areas associated to points 1, 3, 5, 6 and 7 should be located far from TiO_2 agglomerates (i.e. a zone with low dielectric permittivity in figure 4). *(ii)* A quick decrease of the V_{mn} versus time (orange curve in figure 7(b)) is significant of a rapid transport of charge in the bulk of NC film. This rapid charge dissipation is attributed to the presence of TiO_2 agglomerates near charges and probably associated to areas with high dielectric permittivity (figure 4). To quantify such a phenomenon, an insulating quality parameter Q_{insul} has been be defined as

$$Q_{insul} = \frac{n_{SiO_2}}{Z} \tag{3}$$

Where n_{SiO_2} corresponds to the number of $V_{nm} = f(t)$ curves which presents the same dynamics as SiO_2 (blue curves in figure 7) and Z the number of analyzed areas (here Z = 8). In the case of N = 15, $n_{SiO_2} = 5$ and the insulating quality parameter Q_{insul} is 62.5%.

The same phenomenon is observed for N = 20 with an insulating quality parameter Q_{insul} of 50%. For N = 30, a quick decrease of V_{mn} versus time after injection is observed in all injected conditions. Consequently, the insulating quality parameter Q_{insul} is equal to zero.

4. Discussion

To study the influence of the TiO_2 NPs dispersed in the SiO_2 matrix on the dielectric properties of the NC films, relative dielectric permittivity, charges injection and transport have been investigated at nanoscale.

For further interpretation of the relative dielectric permittivity ε_r values, the effective dielectric permittivity measured by EFM (i.e. the mean value over 0.25 μm x 1 μm surface) was plotted as a function of the content of TiO_2 nanoparticles by volume estimated by ellipsometry. As expected, the relative dielectric permittivity is increasing with the TiO_2 NPs content. This relationship could be modeled by several equations and we selected three of them:

- The mixed law that is the simplest equation and corresponds to a volume-average approach. In this model, the effective relative dielectric permittivity of the NC films can be expressed by

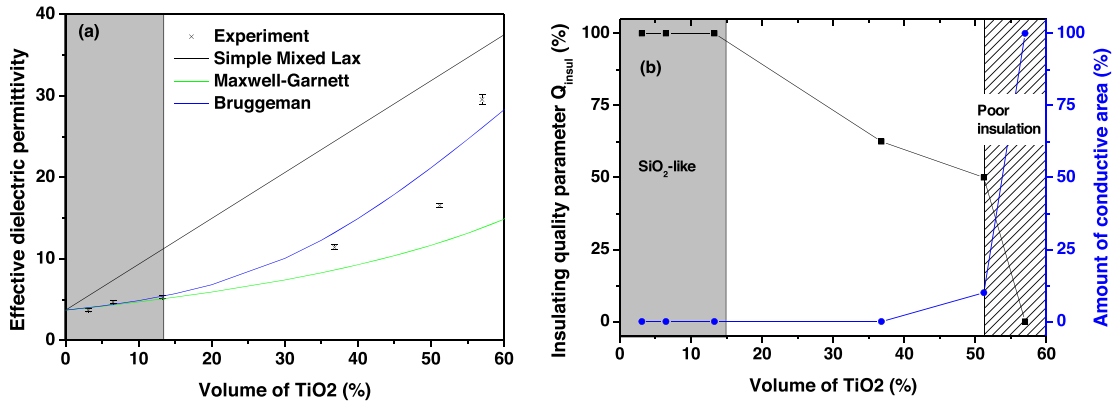

Figure 8. Evolution of the effective dielectric permittivity (error bars are indicated) (a) and the percentage of conductive area (C-AFM) and the insulating quality parameter Q_{insul} (KPFM) with the fraction of TiO_2 by volume (b).

$$\varepsilon_{eff} = \varphi_{SiO_2} \quad \varepsilon_{SiO_2} + \varphi_{TiO_2} \quad \varepsilon_{TiO_2} \tag{4}$$

Where φ_{SiO_2} (φ_{TiO_2}) is the fraction of SiO_2 (or TiO_2) by volume and ε_{SiO_2} (ε_{TiO_2}) is the relative dielectric permittivity of SiO_2 (or TiO_2).

According to equation (4), the relative dielectric permittivity of the NC should increase sharply for low fraction by volume of the nanofiller, as TiO_2 permittivity is one order of magnitude higher than the SiO_2 one. Many studies, reported in the literature, emphasize that the dielectric permittivity of heterostructures is poorly taken into account [39].

- The Maxwell-Garnet theory, which is based on the mean field approximation of a single spherical inclusion embedded in a homogeneous matrix [40, 41]. This model assumes that there is no interactions between inclusions and their respective electrical fields and the matrix. Hence, this model is only valid for a small quantity of NPs in the matrix. The effective relative dielectric permittivity is expressed by

$$\varepsilon_{eff} = \varepsilon_{SiO_2} \frac{\epsilon_{TiO_2}(1 + 2\varphi_{TiO_2}) - 2\varepsilon_{SiO_2}(\varphi_{TiO_2} - 1)}{\varepsilon_{SiO_2}(2 + \varphi_{TiO_2}) + \varepsilon_{TiO_2}(1 - \varphi_{TiO_2})} \tag{5}$$

- The Bruggeman model is also a mean field model but more adapted to high fraction of NC by volume [41]. In that study, NPs are assumed to be dispersed in the effective medium including matrix and the other NPs. Therefore, the interaction with all other particles is taken into account. The effective relative dielectric permittivity is expressed by

$$\varphi_{SiO_2} \frac{\varepsilon_{SiO_2} - \varepsilon_{eff}}{\varepsilon_{SiO_2} + 2\varepsilon_{eff}} + \varphi_{TiO_2} \frac{\varepsilon_{TiO_2} - \varepsilon_{eff}}{\varepsilon_{TiO_2} + 2\varepsilon_{eff}} = 0 \tag{6}$$

In the following, the relative dielectric permittivity of SiO_2 is fixed to 3.8. Concerning the relative dielectric permittivity of TiO_2 anatase, various values are reported in the literature ranging from 48 to 90 for powder [42] and PECVD thin films [8], respectively. In this study, we fixed the TiO_2 dielectric permittivity to 60 (value close to those of red spot in figure 4(h)).

Figure 8(a) shows the evolution of the effective dielectric permittivity, which corresponds to the mean value of the relative dielectric permittivity map probed by EFM (figure 4), as a function of the TiO_2 fraction φ_{TiO2} by volume. We observe that the effective dielectric permittivity increase with the TiO_2 fraction by volume is not linear. For all fraction by volume, the simple mixed law overestimates the effective dielectric permittivity. For $\varphi_{TiO2} \leqslant 14\%$, the Maxwell-Garnet and Bruggeman laws are in good agreement with the experimental data and validate thus the hypothesis of a diluted medium with low amount of NPs and no agglomerates. For φ_{TiO2} above 14%, the experimental results agree well with the Bruggeman law meaning that under electric field, electrostatic interactions take place between nanoparticles due to high TiO_2 fraction by volume and lead to the formation of agglomerates.

All the results of this study demonstrate that the fraction of TiO_2 NPs by volume has a strong impact on dielectric properties of TiO_2 in SiO_2 NC. To get deeper understanding on this impact, the amount of conductive surface determined by C-AFM and the insulation quality factor Q_{insul} determined by KPFM are plotted as a function of the TiO_2 volume fraction (figure 8(b)). Below 14% of TiO_2 fraction by volume ($N \leqslant 10$), the NC

Table 1. Comparison between high-k materials, nanolaminates (NL) and TiO_2 in SiO_2 NC dielectric thin film properties in term of relative dielectric permittivity, leakage current density J and equivalent Oxide Thickness (EOT). Leakage current is obtained either by C-AFM(*) (collection surface estimated to 2 10^{-2} μm^2) or by macroscale measurement(**).

	Dielectric material	ε_r	EOT (nm)	J (A.cm^{-2})	Applied electric field (V.nm^{-1})	Reference
NC	37% TiO_2 in SiO_2	11	17.7	$< 4\ 10^{-4}$ (*)	0.56	This study
	51% TiO_2 in SiO_2	17	11.5	$3\ 10^{-2}$ (*)	0.8	
	57% TiO_2 in SiO_2	30	6.5	$12\ 10^{-2}$ (*)	0.36	
High-k	Y_2O_3	15	15.6	10^{-7} (**)	0.2	Xu *et al* [43]
	a-$LaAlO_3$	16	0.9	10^{-2} (**)	0.01	Pelloquin [44]
	HfO_2	25	1.5	10^{-7} (**)	0.1	Robertson [18]
NL	Ta_2O_5-HfO_2	12	3.25	$2\ 10^{-7}$ (**)	0.1	Zhang [12]
	ZrO_2-HfO_2	14	3.2	$2.6\ 10^{-8}$ (**)	0.1	Zhang [12]
	VO_2-SiO_2	5.42	70	10^{-7} (**)	0.01	Sun [11]

films exhibit a surface morphology and dielectric properties similar to SiO_2 one. Indeed, the surface roughness is extremely small (figure 2(e)), no leakage current is measured and the charge injection and transport exhibit the same dynamics than SiO_2. Such characteristics are significant for well-dispersed TiO_2 NPs in the SiO_2 matrix. This high dispersion is in very good agreement with TEM images. Hence, the dielectric permittivity evolution is well fitted by Maxwell-Garnett law (i.e. dilute medium hypothesis). In such range of NPs contents, the relative dielectric permittivity increases with the TiO_2 volume fraction without affecting the insulating properties of the matrix.

For the 37% TiO_2 NPs content (figure 8), the SiO_2 matrix remains enough insulating with a low conduction conversely with an increased relative dielectric constant of 11 (table 1). In addition, we should notice that, in our work, the leakage current is in the 10^{-4} range ($<4\ 10^{-4}$ A cm^{-2}, see first line in tables 1), i.e. a rather low value considering the value of the applied electrical field, which is higher by almost a factor 6 as compared to results from literature (lower part of table 1).

For a TiO_2 fraction by volume between 37% and 57% ($15 \leqslant N \leqslant 20$), the NC films roughness increases and the dielectric properties are different from SiO_2. Accordingly, the apparent dielectric permittivity (figure 8(a)) and the conductive area surface (figure 8(b)) are increased. Moreover, the insulating quality factor Q_{insul} decreases. As said previously, considering deposition condition with higher N implies that the injector of the TiO_2 colloidal solution is open more often allowing thus the incorporation of a larger amount of solution in the plasma and thus increase of TiO_2 content injected per minute. Actually, when the TiO_2 volume fraction increases, the distance between TiO_2 NPs is decreasing and promotes NPs agglomerates. As TiO_2 NPs exhibit higher conduction than silica matrix, the decreasing of distance between nanoparticles and/or the formation of agglomerates favors charge transport and leads to an increase of the leakage current. The insulating properties of these NC materials are worsened compared to SiO_2 ones but remain suitable. For a TiO_2 fraction of 57 vol%, as TiO_2 is the majority in the NC film, the number of agglomerates becomes important leading to high leakage current, weak amount of trapped charges and quick charge dissipation rate. In this context, one way to improve dielectric properties of TiO_2 in SiO_2 NC films would be to improve the nanoparticles dispersion in fraction by volume in the 32%–52% range.

To conclude, for MIM applications, table 1 gathers values of relative dielectric permittivity and current density for TiO_2 in SiO_2 NC films with those of classical high-k material and nanolaminates (NL). The Equivalent Oxide Thickness (EOT) is calculated using the following equation [18]:

$$EOT = d_D \frac{\varepsilon_{SiO_2}}{\varepsilon_D} \tag{6a}$$

Where d_D is the film thickness and ε_D the dielectric permittivity of the thin dielectric layer.

First, these results emphasize that TiO_2 in SiO_2 NC films allow to reach similar dielectric permittivity than classical high-k materials. Considering leakage current, the comparison is not immediate since macroscale measurement leads to current mean value for large size electrodes (few mm^2) whereas C-AFM gives access to local current values highlighting thus heterogeneity. However, considering an analyzed surface collection of 2 10^{-2} μm^2 a current density could be estimated. Finally, current density values obtained for TiO_2 in SiO_2 NC make them alternative candidates to reference high-k materials to develop MIM structures.

In addition, the comparison of TiO_2 in SiO_2 NC films investigated in this study with TiO_2-SiO_2 nanolaminates is not immediate since dielectric properties of the later are rarely reported in the literature. Indeed, TiO_2-SiO_2 nanolaminates are mainly studied for optical devices applications [33]. However, our TiO_2 in SiO_2 NC films NC films exhibit similar dielectric permittivity to those of laminates classically reported in the literature [15]. The comparison in term of leakage current is not easy as nanolaminates include a top and/or

bottom insulating layer (i.e. SiO_2 layer with thickness ranging from 2 nm to 10 nm) that could limit both charge injection and transport [11–13, 15]. Based on the present study, TiO_2 in SiO_2 NC appear promising for MIM applications.

5. Conclusion

In this paper, the dielectric properties of TiO_2 in SiO_2 NC films are investigated by several techniques derived from AFM, namely relative dielectric permittivity, charges injection and transport. The TiO_2 in SiO_2 NC films are synthetized by an advanced hybrid aerosol-PECVD method based on direct liquid injection of a colloidal solution in an O_2 / HMDSO low-pressure plasma. This technique allows an accurate tuning of the TiO_2 NPs fraction by volume (from 2% to 57%) while controlling the NPs dispersion in the matrix. Results demonstrate that the NPs fraction by volume has a large impact on nanocomposite dielectric permittivity. For low TiO_2 content (less than 14% by vol.), the dielectric properties are similar to silica one. Indeed, the relative dielectric permittivity can be increased up to 4.7 while maintaining the silica insulating properties and surface roughness. For middle range TiO_2 content (i. e. 15%–37% by vol.), the relative dielectric permittivity is strongly increased up to 11 for 37% TiO_2 by volume. In that case, few NPs agglomerates are observed along with a slight increase of the surface roughness. Moreover, the presence of small NPs agglomerates tends to slightly worsen the electrical insulating properties (i.e. charge transport dynamic is favored). At high concentration of TiO_2 NPs (i.e. above 40% by vol.), the quantity of NPs agglomerates becomes important, which increases strongly the leakage current and limits charges trapping. However, the dielectric properties of TiO_2 in SiO_2 NC films, with 37% TiO_2 by volume, appear very challenging to replace high-k materials in MIM-capacitor. The next step will be to optimize the nanoparticles dispersion in the SiO_2 matrix and further investigate their dielectric performances in MIM devices.

Acknowledgments

This work was financially supported by the French GDR SEEDS.

Data availability statement

All data that support the findings of this study are included within the article (and any supplementary files).

ORCID iDs

C Villeneuve-Faure https://orcid.org/0000-0002-7959-2912
M Mitronika https://orcid.org/0000-0002-2918-2579
L Boudou https://orcid.org/0000-0001-5339-2042
W Ravisy https://orcid.org/0000-0003-3705-139X
M P Besland https://orcid.org/0000-0002-2680-2402
M Richard-Plouet https://orcid.org/0000-0002-7871-2919
A Goullet https://orcid.org/0000-0001-5411-4351

References

[1] Jenkins M *et al* 2019 Review—beyond the highs and lows; a perspective on the future of dielectrics research for nanoelectronic devices *ECS J. Solid State Sci. Technol.* **8** N159
[2] Yota J, Shen H and Ramanathan R 2013 Characterization of atomic layer deposition HfO_2, Al_2O_3, and plasma-enhanced chemical vapor deposition Si_3N_4 as metal–insulator–metal capacitor dielectric for GaAs HBT technology *J. Vac. Sci. Technol. Vac. Surf. Films* **31** 01A134
[3] Fan B, Liu F, Yang G, Li H, Zhang G, Jiang S and Wang Q 2018 Dielectric materials for high-temperature capacitors *IET Nanodielectric* **1** 32
[4] Jeon W 2020 Recent advances in the understanding of high-k dielectric materials deposited by atomic layer deposition for dynamic random-access memory capacitor applications *J. Mat. Res.* **35** 775
[5] Bertaud T, Blonkowski S, Bermond C, Vallée C, Gonon P, Gros-Jean M and Fléchet B 2010 Frequency effect on voltage linearity of ZrO_2-based RF metal–insulator–metal capacitors *IEEE Electron Device Lett.* **31** 114
[6] Yim K, Yong Y, Lee J, Lee K, Nahm H H, Yoo J, Lee C, Hwang C S and Han S 2015 Novel high-*k* dielectrics for next-generation electronic devices screened by automated *ab initio* calculations, *NPG Asia Mater.* **7** e190
[7] Khan M S, Kim H J, Taniguchi T, Ebina Y, Sasaki T and Osada M 2017 Layer-by-layer engineering of two-dimensional perovskite nanosheets for tailored microwave dielectrics *Appl. Phys. Express* **10** 091501

[8] Mitronika M, Villeneuve-Faure C, Massol F, Boudou L, Ravisy W, Besland M P, Goullet A and Richard-Plouet M 2021 TiO_2-SiO_2 mixed oxide deposited by low pressure PECVD: insights on optical and nanoscale electrical properties *Appl. Surf. Sc.* **541** 148510

[9] Li W, Auciello O, Premnath R N and Kabius B 2010 Giant dielectric constant dominated by Maxwell–Wagner relaxation in Al_2O_3/TiO_2 nanolaminates synthesized by atomic layer deposition *Appl. Phys. Lett.* **96** 162907

[10] Guan H and Jiang C 2018 Study on the physical and leakage current characteristics of an optimized high-k/InAlAs MOS capacitor with a HfO_2–Al_2O_3 laminated dielectric *Coating* **8** 417

[11] Sun Y *et al* 2018 Thermally tunable VO_2-SiO_2 nanocomposite thin-film capacitors *J. Appl. Phys.* **123** 114103

[12] Zhang H, Solanki R, Roberds B, Bai G and Banerjee I 2000 High permittitivty thin film nanolaminates, *J. Appl. Phys.* **87** 1921

[13] Zhong L, Weston L D, Capbell S A and Gladfelter W L 2006 Atomic layer deposition, characterization and dielectric properties of HfO_2/SiO_2 nanolaminates and comparisions with their homogeneous mixtures *Chem. Vap. Deposition* **12** 143

[14] Patil S R, Barhate V N, Patil V S, Agrawal K S and Mahajan A M 2022 The effect of post-deposition annealing on the chemical, structural and electrical properties of $Al/ZrO_2/La_2O_3/ZrO_2/Al$ high-k nanolaminated MIM-capacitors *J. Mater. Sci., Mater. Electron.* **33** 11227

[15] Azardmanjiri J, Berndt cc, Wang J, Kapoor A, Srivastava V K and Wen C 2014 A review on hybrid nanolaminate materials synthesized by deposition techniques for energy storage application, *J. Mater. Chem.* **2** 3695

[16] O'Neil D, Bowman R M and Gregg J M 2000 Dielectric enhancement and Maxwell–Wagner effects in ferroelectric superlattice structures *Appl. Phys. Lett.* **77** 1520

[17] Chen F C, Chu C W, He J and Yang Y 2004 Organic thin-film transistors with nanocomposite dielectric gate insulator *Appl. Phys. Lett.* **85** 3295

[18] Robertson J 2004 High dielectric constant dielectric *Eur. Phys. J. Appl. Phys.* **28** 265

[19] Charitidis C A, Georgiou P, Koklioti M A, Trompeta A-F and Markakis V 2014 Manufacturing nanomaterials: from research to industry *Manuf. Rev.* **1** 11

[20] Larouche S, Szymanowski H, Klemberg-Sapieha J E, Martinu L and Gujrathi S C 2004 Microstructure o plasma-deposited SiO_2/TiO_2 optical films *J. Vac. Sci. Technol. A* **22** 1200

[21] Makasheva K, Villeneuve-Faure C, Bonafos C, Laurent C, Pugliara A, Despax B, Boudou L and Teyssedre G 2016 Dielectric engineering of nanostructured layers to control the transport of injected charges in thin dielectrics *IEEE Trans. Nanotechnol.* **15** 839–48

[22] Li D, Elisabeth S, Granier A, Carette M, Goullet A and Landesman J-P 2016 Structural and optical properties of PECVD TiO_2–SiO_2 mixed oxide films for optical applications *Plasma Processes Polym.* **13** 918

[23] Mitronika M, Profili J, Goullet A, Gautier N, Stephant N, Stafford L, Granier A and Richard-Plouet M 2021 TiO_2 –SiO_2 nanocomposite thin films deposited by direct liquid injection of colloidal solution in an O_2 /HMDSO low-pressure plasma *J. Phys. D: Appl. Phys.* **54** 085206

[24] Karpinski A, Berson S, Terrisse H, Mancini-Le Granvalet M, Guillerez S, Brohan L and Richard-Plouet M 2013 Anatase colloidal solutions suitable for inkjet printing: Enhancing lifetime of hybrid organic solar cells *Sol. Energy Mater. Sol. Cells* **116** 27

[25] Profili J, Levasseur O, Koronai A, Stafford L and Gherardi N 2017 Deposition of nanocomposite coatings on wood using cold discharges at atmospheric pressure *Surf. Coat. Technol.* **309** 729–37

[26] El Kass M, Brohan L, Gautier N, B´echu S, David C, Lemaitre N and Berson S 2017 and Richard-Plouet M *ChemPhysChem* **18** 2390–6 TiO2 anatase solutions for electron transporting layers in organic photovoltaic cells

[27] Bousquet A, Bursikova V, Goullet A, Djouadi A, Zajickova L and Granier A 2006 Comparison of structure and mechanical properties of SiO_2-like films deposited in O_2/HMDSO pulsed and continuous plasmas *Surf. Coat.Technol.* **200** 6517–21

[28] Mitronika M, Profili J, Goullet A, Stafford L, Granier A and Richard-Plouet M 2020 Modification of the optical properties and nano-crystallinity of anatase TiO_2 nanoparticles thin film using low pressure O_2 plasma treatment *Thin Solid Films* **709** 138212

[29] Riedel C, Arinero R, Tordjeman P ,, Ramonda M, Lévêque G, Schwartz G A, De Oteyza D G, Alegria A and Colmenero J 2009 Determination of the nanoscale dielectric constant by means of a double pass method using electrostatic force microscopy *J. Appl. Phys.* **106** 024315

[30] Houssat M, Villeneuve-Faure C, Lahoud Dignat N and Cambronne J P 2021 Nanoscale mechanical and electrical characterization of the interphase in polyimide/silicon nitride nanocomposites *Nanotechnology* **32** 425703

[31] Villeneuve-Faure C, Makasheva K, Boudou L and Teyssedre G 2016 Charge injection in thin dielectric layers by atomic force microscopy: influence of geometry and material work function of the AFM tip on the injection process *Nanotechnology* **27** 245702

[32] Miquelot A *et al* 2021 In- and out-plane transport properties of chemical vapor deposited TiO_2 anatase films, *J. Mater. Sci.* **56** 10458

[33] Ghazaryan L, Handa S, Schmitt P, Beladiya V, Roddatis V, Tünnermann A and Szeghalmi A 2020 Structural, optical, and mechanical properties of TiO_2 nanolaminates *Nanotechnology* **32** 095709

[34] Wang S, Fan L, Luo Z, Li J, Li L, He J and Li Q 2022 Insight into the experimental error in the mapping of the electrical properties with electrostatic force microscopy *Langmuir* **38** 8543

[35] Van de Hofstadt M, Fabregas R, Biagi M, Fumigalli L and Gomila G 2016 Nanoscale dielectric microscopy of non-planar samples by lift-mode electrostatic force microscopy *Nanotechnology* **27** 405706

[36] Dianoux R, Smilde H J H, Marchi F, Buffet N, Mur P, Comin F and Chevrier J 2005 Kinetic roughening of charge spreading in a two-dimensional silicon nanocrystal network detected by electrostatic force microscopy *Phys. Rev. B* **71** 125303

[37] Han B, Chang J, Song W, Sun Z, Yin C, Lv P and Wang X 2019 Study on micro interfacial charge motion of polyethylene nanocomposite based on electrostatic force microscope *Polymers* **11** 2035

[38] Mortreuil F, Boudou L, Makasheva K, Teyssedre G and Villeneuve-Faure C 2021 Influence of dielectric layer thickness on charge injection, accumulation and transport phenomena in thin silicon oxynitride layers: a nanoscale study *Nanotechnology* **32** 065706

[39] Brosseau C 2006 Modelling and simulation of dielectric heterostructures: A physical survey from an historical perspective *J. Phys. D: Appl. Phys.* **39** 1277–94

[40] Maxwell Garnett J C 1904 Colours in metal glasses and in metallic films *Philos. Trans. R. Soc. A Math. Phys. Eng. Sci.* **203** 385–420

[41] Choy T C 1999 *Effective Medium Theory: Principles and Applications.* (International Monograph in Physics, Oxford Science Publication)

[42] Harris L A 1980 Titanium dioxide hydrogen detector *J. Electrochem. Soc.* **127** 2657

[43] Xu H, Ding X, Qi J, Yang X and Zhang J 2021 A study on solution-processed Y_2O_3 films modified by atomic layer deposition Al_2O_3 as dielectrics in ZnO thin film transistor *Coatings* **11** 969

[44] Pelloquin S, Saint-Girons G, Baboux N, Albertini D, Hourani W, Penuelas J, Grenet G, Plossu C and Hollinger G 2013 $LaAlO_3$/Si capacitors: comparison of different molecular beam deposition conditions and their impact on electrical properties *J. Appl. Phys.* **113** 034106